Dalton Transactions

Inorganic Clusters as Metalloligands: Ligand Effects on the Synthesis and Properties of Ternary Nanopropeller Clusters

Journal:	*Dalton Transactions*
Manuscript ID	DT-ART-07-2020-002416.R1
Article Type:	Paper
Date Submitted by the Author:	23-Aug-2020
Complete List of Authors:	Kephart, Jonathan; University of Washington, Department of Chemistry Boggiano, Andrew; University of Washington, Chemistry Kaminsky, Werner; University of Washington, Chemistry Velian, Alexandra; University of Washington, Chemistry

Paper

Inorganic Clusters as Metalloligands: Ligand Effects on the Synthesis and Properties of Ternary Nanopropeller Clusters

Jonathan A. Kephart,[a] Andrew C. Boggiano,[a] Werner Kaminsky,[a] and Alexandra Velian *[a]

Received 00th January 20xx,
Accepted 00th January 20xx

DOI: 10.1039/x0xx00000x

Redox-active multimetallic platforms with synthetically addressable and hemilabile active sites are attractive synthetic targets for mimicking the reactivity of enzymatic co-factors toward multielectron transformations. To this end, a family of ternary clusters featuring three edge metal sites anchored on a [Co_6Se_8] multimetallic support via amidophosphine ligands are a promising platform. In this report we explore how small changes in the stereoelectronic properties of these ligands alter [Co_6Se_8] metalloligand formation, but also substrate binding affinity and strength of the edge/support interaction in two new ternary clusters, $M_3Co_6Se_8L_6$ (M = Zn, Fe; $L^{(-)}$ = $Ph_2PN^{(-)i}Pr$). These clusters are characterized extensively using a range of methods, including single crystal X-ray diffraction, electronic absorption spectroscopy and electrochemistry. Substrate binding studies reveal that $Fe_3Co_6Se_8L_6$ resists coordination of larger ligands like pyridine or tetrahydrofuran, but binds to the smaller ligand CN^tBu. Additionally, investigations in the synthesis of new [Co_6Se_8] metalloligands using two aminophosphines, $Ph_2PN(H)^iPr$ (L^H) and $^iPr_2PN(H)^iPr$ led to the synthesis and characterization of $Co_6Se_8L^H_6$, as well the smaller clusters $Co_4Se_2(CO)_6L^H_4$, $Co_3Se(\mu_2\text{-}PPh_2)(CO)_4L^H_3$, and $[Co(CO)_3(^iPr_2PN(H)^iPr)]_2$. Cumulatively, this study expands our understanding on the effect of the stereoelectronic properties of aminophosphine ligands in the synthesis of cobalt chalcogenide clusters, and, importantly on modulating the push-pull dynamic between the [Co_6Se_8] support, the edge metals and incoming coordinating ligands in ternary $M_3Co_6Se_8L_6$ clusters.

Introduction

Multimetallic clusters play a critical role in many enzymatic transformations, including nitrogen fixation and oxygen evolution among other challenging multielectron catalytic sequences.[1] Key features that enable their reactivity include their overall structural plasticity, which allows flexible active site conformations, and intracluster intermetallic cooperativity to facilitate multielectron processes.[2,3] Replicating enzymatic reactivity in synthetic clusters has been an area of intense research, and numerous synthetic platforms have been explored to achieve this. Figure 1a displays a small selection of site differentiated clusters, including the heterocubane $[Mo(L_2)Fe_3S_4Cl_3]^{2-}$ (L_2^{2-}= tetrachlorocatecholate),[4] the polyoxovanadate $FeV_5O_6(OCH_3)_{12}$,[5] and the tetrametallic oxo cluster $MnFe_3(\mu_4\text{-}O)L_3L'$ (L = phenylpyrazolate; L' = 1,3,5-triarylbenzene based ligand).[6] These platforms illustrate instances in which the active site is rigidly embedded in a redox-active polymetallic framework that modulates its stoichiometric and even catalytic reactivity. Instead, an active site bound in a hemilabile fashion to a polymetallic framework might better replicate the structural plasticity of enzymatic clusters and lead to higher reactivity, but achieving this requires synthetic innovations. Successful strategies to install a "dangler" metal on an inorganic cluster have been developed, especially in the context of modelling the oxygen evolving complex.[7–10] Figure 1b includes such an example, the

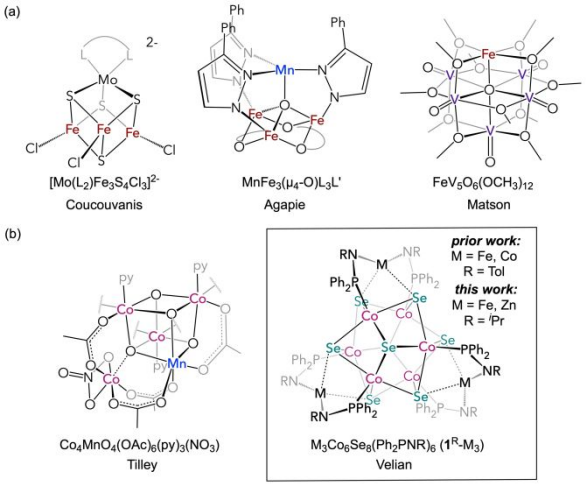

Figure 1. Heterometallic clusters featuring (a) active sites rigidly embedded within the polymetallic framework, (b) dangler sites tethered at the cluster surface.

[a] University of Washington, Department of chemistry, Seattle, WA, USA, 98195.
Electronic Supplementary Information (ESI) available: Experimental procedures and characterization data, including CIF files for $\mathbf{1}^{iPr}$-H_6, $[\mathbf{1}^{iPr}\text{-}H_6][PF_6]$, **2**, **3**, **4**, $\mathbf{1}^{iPr}$-Zn_3, and $\mathbf{1}^{iPr}$-Fe_3 are available in the Electronic Supplementary Information (ESI). See DOI: 10.1039/x0xx00000x.

heterocubane $Co_4MnO_4(OAc)_6(py)_3(NO_3)$ (Ac = acetate) featuring a dangling Co(II) subsite.[7] Our group recently introduced a modular strategy to install active sites that interact in a hemilabile fashion with a redox-active multimetallic platform, and demonstrated these designer clusters are catalytically competent.[11,12] The ternary nanocluster $Fe_3Co_6Se_8(Ph_2PNTol)_6$ (**1**^{Tol}-Fe_3, Figure 1b) features three Fe edge sites, each anchored to a $[Co_6Se_8]$ cluster core by two amides and two hemilabile Fe...Se interactions. This cluster concept is highly modular, as the surface binding sites are poised to host other metals (e.g. cobalt),[12] and the stereoelectronic properties of the amidophosphine ligands can be easily tuned.[13]

In our initial report,[11] we discovered that the strength of the Fe...Se interaction is redox-modulated. For example, monoreduction of **1**^{Tol}-Fe_3, which effectively localizes an extra electron on the polymetallic cobalt core, increases the Fe...Se interaction strength and lowers the edge sites affinity for ligands to zero. Here, we set out to explore further this push-pull relation between the cluster support, the edge site and the incoming substrates, by probing how the nature of the edge/core interaction changes when ligand coordination is sterically blocked at the edge sites. To achieve this, we chose two aminophosphines that are slightly bulkier and also more electron rich than $Ph_2PN(H)Tol$, namely $^{i}Pr_2PN(H)iPr$ and $Ph_2PN(H)^{i}Pr$.[14,15] To our surprise, we found that subtle changes in stereoelectronic properties of the aminophosphine not only affect ligand coordination at the edge sites and the electronic structure of the ternary clusters, but have long ranging consequences in the synthesis of the targeted $[Co_6Se_8]$ metalloligands, altering optimal reaction conditions and even favoring formation of smaller clusters. We report here our detailed findings on both fronts, including the synthesis and characterization of the two ternary clusters $M_3Co_6Se_8L_6$ (**1**^{iPr}-M_3; M = Zn, Fe; L = $Ph_2PN^{i}Pr$), the metalloligand $Co_6Se_8L^H_6$ (**1**^{iPr}-H_6; L^H = $Ph_2PN(H)^{i}Pr$), as well as the smaller clusters $Co_4Se_2(CO)_6L^H_4$ (**2**) and $Co_3Se(\mu_2\text{-}PPh_2)(CO)_4L^H_3$ (**3**), and $[Co(CO)_3(^{i}Pr_2PN(H)^{i}Pr)]_2$ (**4**).

Results and Discussion

Ligand effects in the synthesis of a $[Co_6Se_8]$ metalloligand

Several protocols are available to synthesize molecular cobalt chalcogenide Chevrel-type clusters. The first reported syntheses of $Co_6Q_8L_6$ (Q = S, Se; L = PPh_3) clusters relied on the use of silylated or anionic chalcogen sources, such as $Se(SiMe_3)_2$ and Na_2S, in conjunction with the phosphine-bound cobalt halide precursor, $CoCl_2(PPh_3)_2$.[16–18] A more convenient synthetic route that circumvents the experimental challenges associated with manipulating reactive chalcogen sources involves using instead a Co(0) source, elemental chalcogen, and phosphine ligands in different ratios.[19–21] For example, to produce $Co_6Q_8L_6$ clusters, stoichiometric $Co_2(CO)_8$ is treated with excess of both the chalcogen and the phosphine (≥12 equiv),[20–23] whereas stoichiometric tellurium and excess phosphine are used to synthesize the more electron rich $Co_6Te_8L_6$ variants.[19,20,24] Empirically, it has been found that using excess chalcogen alone shifts the distribution of products toward the formation of partially carbonylated clusters $Co_6Se_8(CO)_xL_{6-x}$.[25]

While the details of the mechanism by which Chevrel-type clusters assemble are not well understood, the phosphine is proposed to play a critical role in their synthesis. In addition to binding to Co, the phosphine effectively functions as a chalcogen transfer reagent.[24] Empirically, we note the identity of the phosphine has a pronounced influence over the cluster formation process. For example, replacing a single ethyl group in PEt_3 with a bulkier and less electron rich group (*i.e.* 4-bromophenyl or 9-ethynylphenanthroline) results in significantly longer reaction times.[20–22] The stereoelectronic nature of the phosphine stands to alter the numerous equilibria involved in the formation of $[Co_6Se_8]$ clusters, altering both the rates of formation of different intermediates and the final distribution of products. Steric bulk considerations seem an especially important factor: while no $Co_6Se_8L_6$ clusters have been reported to form with bulkier phosphines (*i.e.* $P^{i}Pr_3$), phosphines of very different donor-acceptor properties (e.g. PEt_3 and PPh_3)[26] have been successfully used to produce them.

In this study we find that while the aminophosphine $Ph_2PN(H)^{i}Pr$ (L^H) yields the $[Co_6Se_8]$ cluster **1**^{iPr}-H_6, the related ligand $^{i}Pr_2PN(H)^{i}Pr$, completely inhibits its formation, halting the reaction to yield the dimer $[Co(CO)_3(^{i}Pr_2PN(H)^{i}Pr)]_2$ (**4**). Comparing strictly the relative steric bulk for PPh_3, PEt_3, Ph_2PCH_2Ph and $^{i}Pr_2PCH_2Ph$ (the latter two serving as proxies for L^H and $^{i}Pr_2PN(H)^{i}Pr$) using the Tolman cone angles in octahedral coordination environments, we find they steadily increase in the series from 152.0°, 157.8°, 165.5°, to 172.7°, respectively.[14,27] A similar trend in steric profiles is obtained using the percent buried volume method, which estimates values for this parameter between 27.6% and 29.1% for PPh_3, L^H and $Ph_2PN(H)Tol$, and slightly larger for $^{i}Pr_2PN(H)^{i}Pr$, at 31.5%.[15]

Aminophosphine $^{i}Pr_2PN(H)^{i}Pr$ halts cluster formation to Co dimer 4

The stoichiometric reaction of $Co_2(CO)_8$, Se and $^{i}Pr_2PN(H)^{i}Pr$ produced only the Co(0) dimer complex **4** (38% isolated yield), and no other observable cobalt products (Scheme 1). The UV-vis spectrum of this dimer features an absorption band at 377 nm, and infrared analysis reveals the presence of a terminal CO ligand (ν_{CO} = 1943 cm^{-1}). X-ray quality red-orange prismatic crystals of **4** were grown from diethyl ether at –35 °C, allowing for its structural characterization in the solid state. The compound features a long unsupported Co–Co bond (2.6731(6) Å; formal shortness ratio r = 1.16),[28,29] with each Co(0) atom

Scheme 1. Aminophosphine $^{i}Pr_2PN(H)^{i}Pr$ leads to the formation of dimer **4**, and no $[Co_6Se_8]$ cluster.

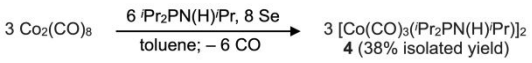

capped by three terminal CO groups and one $^{i}Pr_2PN(H)^{i}Pr$ aminophosphine in an overall trigonal bipyramidal geometry (Figure S29).[30] Similar $[Co(CO)_3(PR_3)]_2$ dimers equipped with a variety of phosphine ligands have been previously isolated, and used as pre-catalysts for the hydroformylation of alkenes.[31,32] **4** is thermally robust, and does not undergo further chemical transformation upon treatment with $SeP^{i}Pr_2N(H)^{i}Pr$ or with elemental selenium in refluxing toluene.

Aminophosphine L^H alters optimal reagent stoichiometry

Having quickly discovered that $^{i}Pr_2PN(H)^{i}Pr$ does not lead to formation of the $[Co_6Se_8]$ cluster under the experimental conditions we sampled, we turned to a close variant of aminophosphine $Ph_2PN(H)Tol$, namely L^H, with a slightly bulkier and more electron rich isopropyl substituent that is spatially removed from the core-binding phosphorous center. To identify a synthetic protocol to prepare $\mathbf{1}^{i\text{Pr}}\text{-}H_6$, we investigated a range of conditions, including stoichiometric reagent ratios, excess L^H, and excess SeL^H, with each variation yielding a different mixture of products (Scheme 2). Refluxing $Co_2(CO)_8$ with excess SeL^H (12 equiv), a protocol successfully yielding a range of $Co_6Se_8(PR_3)_6$ clusters,[20–23] produced instead a mixture of partially carbonylated $Co_6Se_8(CO)_xL^H_{6-x}$ clusters and the [4,2] cluster **2** (Scheme 2a). Refluxing stoichiometric $Co_2(CO)_8$ and Se with excess L^H (12 equiv), a strategy used to prepare $Co_6Te_8(PEt_3)_6$,[20] completely hindered the formation of the $[Co_6Se_8]$ cluster, forming instead a mixture of **2** and **3** (Scheme 1b). Empirically, we found that increasing both the concentration of the reagents and the amounts of phosphine and selenium favored formation of **3**, allowing its isolation and characterization (Scheme 2c). Ultimately, the optimized synthetic protocol for $\mathbf{1}^{i\text{Pr}}\text{-}H_6$ entails refluxing a stoichiometric ratio of $Co_2(CO)_8$, Se, and L^H, followed by addition of excess L^H under continued reflux to convert partially carbonylated products to $\mathbf{1}^{i\text{Pr}}\text{-}H_6$ (Scheme 2d).

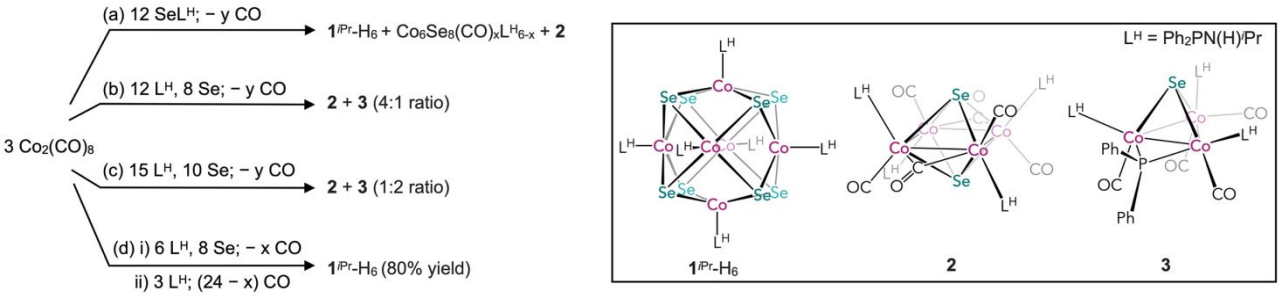

Scheme 2. Effects of the stoichiometry of reagents on the nuclearity and ratio of the cobalt selenide clusters produced in the reaction of $Co_2(CO)_8$, Se, L^H or SeL^H in refluxing toluene.

$[Co_4Se_2]$ cluster 2 and its conversion to $\mathbf{1}^{i\text{Pr}}\text{-}H_6$

Having discovered that the presence of excess phosphine at the onset of the synthesis halts the cluster assembly reaction to mainly **2** (Scheme 2b), we proceeded to isolate it pure. NMR spectroscopy analysis of the crude mixture revealed the presence of SeL^H and L^H. Following their removal using *n*-pentane, **2** was isolated pure as a dark green solid (0.219 g, 24% yield of first crop) by extraction in toluene and subsequent crystallization from THF/*n*-pentane. The single set of proton NMR resonances associated with the aminophosphine ligand are accompanied by a broad singlet in the ^{31}P NMR (82 ppm, $\nu_{1/2}$ = 320 Hz), suggestive of the high symmetry of the complex. UV-vis spectroscopy revealed four broad electronic absorption bands between 329 and 626 nm (Figure 3b), closely matching those of previously reported $Co_4Se_2(CO)_6(P^nBu_3)_4$,[20] and distinct from those of $[Co_6Se_8]$ clusters. The presence of terminal and bridging carbonyl ligands is evident in the infrared spectrum of the main product, with CO stretches at 1927 and 1775 cm^{-1}.

While the combination of spectroscopic characterizations indirectly pointed to the formation of a partially carbonylated $[Co_4Se_2]$ cluster as the main product of the reaction,[24,33] its identity as **2** was confirmed using single crystal X-ray diffraction (Figure 2). Related bicapped, rectangular $[Co_4Se_2]$ clusters, such as $Co_4Se_2(CO)_{10}$ or $Co_4Se_2(CO)_6(P^nBu)_4$, have been previously isolated from the reaction of $Co_2(CO)_8$ with either the more soluble red selenium (1:1 mole ratio), or with a mixture of Se and P^nBu_3 (1:1:4 mole ratio).[20,34] **2** is only the second $[Co_4Se_2]$ cluster to be structurally characterized, with Co…Co and Co…Se distances closely matching its predecessor, $Co_4Se_2(CO)_{10}$.[35] The cluster core features a rectangular plane of Co(I) metals, that is capped on both faces by μ_4-Se ligands (Figure 2b). Interatomic Co…Co distances are observed between 2.54(1) and 2.746(1) Å, indicative of weak Co–Co bonds (formal shortness ratio, r = 1.09, and 1.19, respectively),[28,29] and Co–Se bond lengths average 2.38 Å. The two shortened Co–Co contacts are supported by bridging CO ligands, as indicated by the presence of a 1775 cm^{-1} infrared feature. Each Co metal vertex is also bound by one L^H ligand and one terminal CO. The up/down orientation of these ligands with respect to the plane of the metal ring alternates at each corner of the rectangle, enforcing the overall C_{2v} symmetry of the inorganic unit.

[4,2] clusters, such as $Co_4Se_2(CO)_6(P^nBu_3)_4$ or $Co_4Te_2(CO)_6(PEt_3)_4$, have been shown to thermally convert to the corresponding [6,8] clusters in the presence of excess phosphine and chalcogen.[20,24] To test if **2** is a competent precursor to **1**^{iPr}-H_6, a mixture of **2** (1 equiv), L^H (12 equiv) and selenium (6 equiv) was refluxed in toluene. Mild effervescence and a gradual color change from deep green to red-brown accompanied the reaction (Figure 3). ^{1}H NMR analysis of the crude reaction mixture revealed the clean conversion of the [Co_4Se_2] starting material to **1**^{iPr}-H_6 (Figure S8). The UV-vis absorption spectrum of this mixture bears the tell-tale signs of a [Co_6Se_8] cluster with three strong absorption features at 365, 444 and 505 nm. While excess L^H was found to halt the self-assembly process to the formation of **2**, excess phosphine and Se are necessary to convert this intermediate to the desired species **1**^{iPr}-H_6.

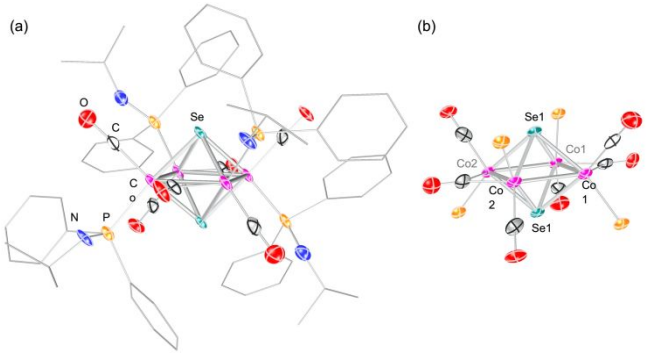

Figure 2. Single crystal X-ray diffraction structure of **2** in full (a), and trimmed to only the inorganic core and the immediate coordination sphere (b). Selected interatomic distances(Å): Co1–Co1 2.54(1), Co1–Co2 2.746(1), Co2–Co2 2.51(1); Co1–Se1 2.386(5), Co2–Se1 2.405(2). Thermal ellipsoids are plotted at 50% probability level. All hydrogen atoms are omitted, and the aminophosphine carbon atoms are plotted as wireframes for clarity.

Isolation of [Co_3Se] cluster 3

Empirically, we discovered that altering the stoichiometry of the reagents to a molar ratio of 6 Co: 10 Se: 15 L^H and increasing the concentration of the reagents led to the preferential formation of the [Co_3Se] cluster **3** over **2** (Scheme 2c). After a solvent workup, the new cluster could be isolated pure as a deep red solid (35% yield) by crystallization from a mixture of toluene and *n*-pentane. Analysis by ^{31}P NMR spectroscopy revealed that the product is desymmetrized, featuring three broad resonances in a 2:1:1 ratio at 82, 89 and 165 ppm ($\nu_{1/2}$ ≈ 370–400 Hz). The signal at 165 ppm is shifted downfield significantly from Co–bound L^H, providing a first clue of the fragmentation incurred by the aminophosphine. This signal is located within a spectral region typical for bridging cobalt phosphido ligands. For example, $Co_2(\mu\text{-}PPh_2)_2(CO)_2(PEt_2Ph)_2$ and $Co_3(\mu_2\text{-}PPh_2)_3(CO)_5(PEt_2Ph)$ exhibit phosphido ^{31}P signals at 176, 199, and 275 ppm, respectively.[36] ^{1}H and ^{13}C NMR spectroscopy analysis indicates the presence of two L^H environments in a 2:1 ratio, along with a separate set of PPh_2 aromatic resonances that corroborate the fragmentation of the P–N bond. Infrared spectroscopy confirmed the presence of only terminal carbonyl ligands, with three CO stretches observed between 1982 and 1918 cm^{-1}. Finally, the UV-vis spectrum contains two broad absorption bands at 369 and 636 nm, distinguished from those typical of [Co_6Se_8] or [Co_4Se_2] clusters (Figure S12).

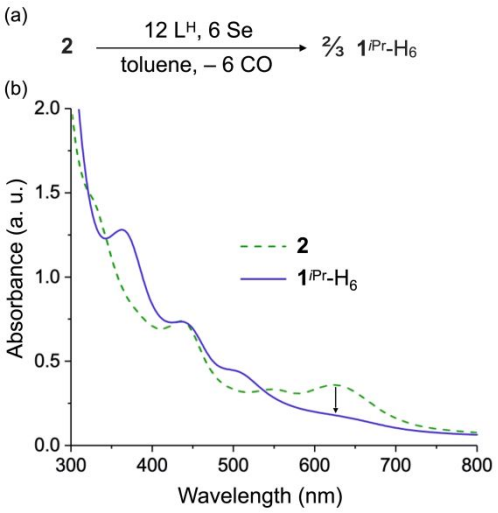

Figure 3. (a) Thermal conversion of **2** to **1**^{iPr}-H_6 in the presence of excess L^H and Se. (b) UV-vis absorption analysis of the reaction mixture before and after the thermal conversion, revealing a clear transition to the absorption profile characteristic of [6,8] clusters.

The product was identified as the novel [Co_3Se] cluster **3** using single crystal X-ray diffraction (Figure 4a). Red needle-shaped crystals were grown via vapor diffusion of diethyl ether into a concentrated THF solution of the compound at 25 °C. The Co_3Se core consists of a triangular Co_3 unit capped by a μ_3-Se atom. The interatomic Co–Co distances, ranging between 2.47(1) and 2.62(1) Å, are again indicative of weak metal-metal bonding interactions (r = 1.07, 1.11, 1.13). A diphenylphosphido ligand, μ_2-PPh_2, formed ostensibly via fragmentation of the aminophosphine P–N bond, bridges between two of the cobalt atoms. The asymmetry of the cluster detected in the infrared and NMR spectra is reflected also in the distribution of the terminal ligands. While each cobalt is hexacoordinate, Co2 and Co3 are terminally bound to one L^H and one CO, whereas the third metal, Co1, is coordinated by an aminophosphine and two CO ligands (Figure 4b).

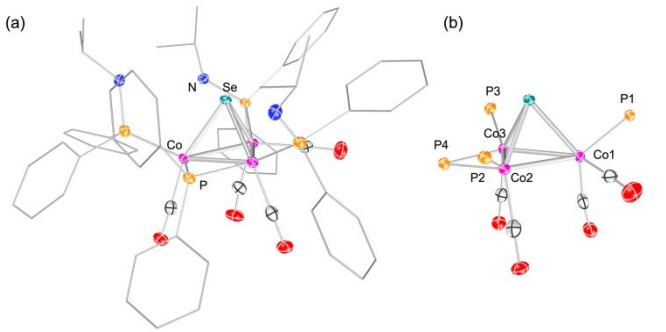

Figure 4. Single crystal X-ray diffraction structure of **3** in full (a), and trimmed to only the inorganic core (b). Selected interatomic distances(Å): Co1–Co2 2.57(2), Co1–Co3 2.62(1), Co2–Co3 2.47(1); Co1–Se1 2.29(1), Co2–Se1 2.30(2), Co3–Se1 2.314(9); Co2–P4 2.179(9), Co3–P4 2.19(1). Thermal ellipsoids are plotted at 50% probability level. All hydrogen atoms and co-crystallizing solvent molecules are omitted. The aminophosphine carbon atoms are plotted as wireframes for clarity.

The structural similarity of [Co_3Se] complexes with the $Co_3(\mu_3\text{-}Se)$ corners of the Co_6Se_8 core suggests they might be intermediates in the formation of Chevrel-type clusters. Inspecting the literature we find that [Co_3Se] clusters that are bound exclusively by L-type ligands[37] are unstable with respect to isolation. For example, $Co_3Se(CO)_9$ decomposes unless stored under carbon monoxide.[34] Molecular orbital considerations have attributed the high reactivity of $Co_3Se(CO)_9$ to the half-occupancy of a tricobalt antibonding orbital.[38] Typically, the inherent instability of such 27 electron, S = 1/2 [Co_3Se] clusters is overcome upon formal mono-oxidation to a 26 electron, diamagnetic cluster by introducing an anionic X-type ligand in the coordination environment of the metal ring.[39] Indeed, there is a plenitude of [Co_3Q] clusters that contain an X-type ligand, such as $Co_3SePh(CO)_8$ or $Co_3S(\mu_2\text{-}S^tBu)(CO)_7$.[39,40] While **3** is the first [Co_3Se] cluster bound by a bridging phosphido, a close [Co_3S] variant, $Co_3S(\mu_2\text{-}PPh_2)(CO)_6(PPh_3)$, has been previously reported. Interestingly, this species forms in the reaction between $Co_2(CO)_8$ with Ph_2PSPh, effectively via the fragmentation of the thiophosphine P–S bond.[41] Here, we hypothesize that if a putative 27 electron [Co_3Se] cluster $Co_3Se(CO)_{9-x}L^H_x$ is formed in the presence of excess aminophosphine, it favors conversion to the observed, and more stable, 26 electron species **3** via activation of the aminophosphine P–N bond and incorporation of the bridging phosphide. The relative susceptibility of the P–N bond toward fragmentation (compared to less reactive P–C bonds), allows here the observation and trapping of an otherwise elusive [Co_3Se] cluster intermediate.

Homoleptic cluster 1^{iPr}-H_6 and its chemical mono-oxidation

Prepared by adding excess L^H (3 equiv) to a refluxing a stoichiometric mixture of $Co_2(CO)_8$, Se, and L^H in toluene (Scheme 2d), $\mathbf{1}^{iPr}$-H_6 is isolated pure in good yield (11.2 g, 80% yield) as a dark red, microcrystalline solid. In solution, $\mathbf{1}^{iPr}$-H_6 exhibits a single set of ^1H NMR resonances for the six aminophosphine ligands, and a broad singlet in the ^{31}P NMR spectrum at 98 ppm. UV-vis absorption analysis in toluene reveals the diagnostic absorption profile anticipated for [Co_6Se_8] clusters, with three broad absorption bands cascading from higher to lower intensity at 365, 444, and 505 nm, respectively.

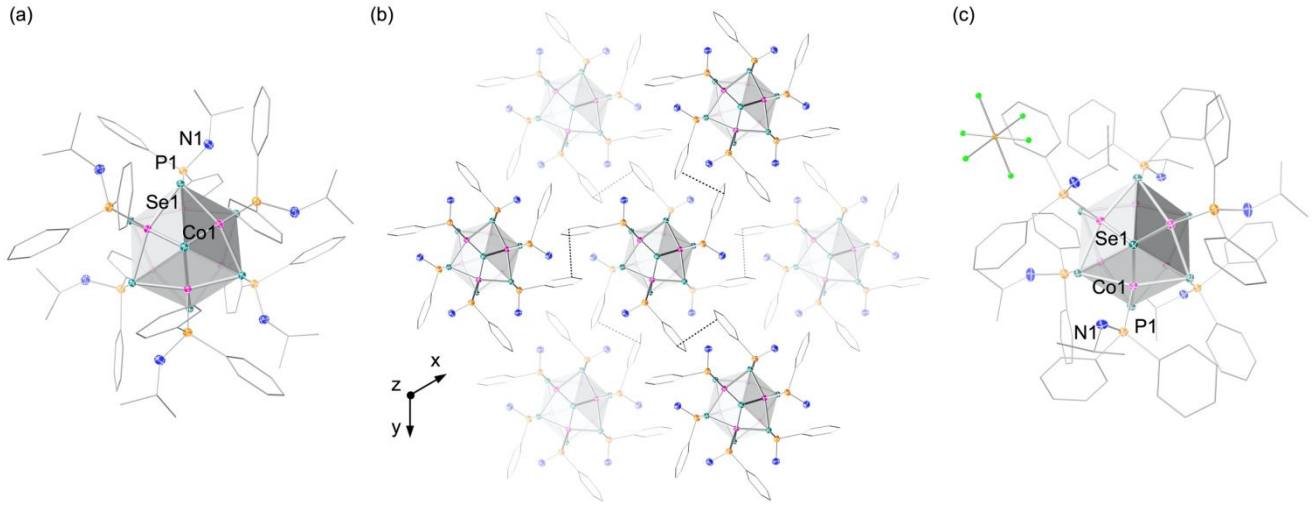

Figure 5. Single crystal X-ray diffraction structure of (a) neutral cluster $\mathbf{1}^{iPr}$-H_6 and (b) its packing in the lattice governed by π-π stacking of phenyl rings, and (c) the mono-oxidized cluster, [$\mathbf{1}^{iPr}$-H_6][PF_6]. Selected interatomic distances (Å): (a) Co1–Se1 2.3334(5), Co1…Co1 2.9961(6), Se1…Se1 5.5081(9), Se2…Se2 5.6655(7); (b) intermolecular Ph…Ph distances 3.547(6); (c) Co1–Se1 2.350(2), Co1–P1 2.164(6), P1–N1 1.672(5). Thermal ellipsoids are plotted at 50% probability level. The aminophosphine carbon atoms are plotted as wireframes, and the atoms in PF_6^- counterion as spheres for clarity. All hydrogen atoms and disorder are omitted.

The homoleptic cluster $\mathbf{1}^{iPr}$-H_6 crystallizes in the trigonal space group $R\bar{3}$ and features a Co_6Se_8 core with pseudo-octahedral symmetry (Figure 5a). All eight trigonal facets of the distorted Co_6 octahedron are capped by μ_3-Se ligands, with Co–Se bond lengths of 2.34 Å (avg.). Each Co metal is bound in a square pyramidal geometry via four μ_3-Se atoms and an aminophosphine ligand. This mixed-valent, formally $(Co^{III})_4(Co^{II})_2$, cluster features nearly equivalent interatomic Co…Co distances, ranging from 2.9390(5) to 2.9961(6) Å.[42] In contrast to the more reduced [Co_3Se] and [Co_4Se_2] congeners, these elongated Co…Co distances indicate the absence of metal-metal bonding (r = 1.29), which is the norm for $Co_6Se_8L_6$ clusters.

Notably, in contrast to $\mathbf{1}^{Tol}$-H_6 and other reported [Co_6Se_8] clusters, the isopropyl derivative $\mathbf{1}^{iPr}$-H_6 has extremely poor solubility in conventional organic solvents post-purification. In fact, dissolving it requires stirring in chlorobenzene (PhCl) at temperatures exceeding 120 °C for at least 1 h. Single crystal X-ray characterization of $\mathbf{1}^{iPr}$-H_6 sheds light on the root cause of its low solubility, revealing that upon crystallization an intermolecular network of π-π interactions is formed (Figure 5b). Each cluster organizes around it a supramolecular octahedron of clusters by engaging one phenyl substituent of each of its aminophosphine ligands in π-π interactions with a phenyl group of a neighbouring cluster.[43] Interestingly, the Co_6Se_8 core is compressed along the z axis, with axial and equatorial Se…Se distances of 5.5081(9) and 5.6655(5) Å, respectively. While this core compression is intriguing, $\mathbf{1}^{Tol}$-H_6 exhibits a similar trend in its Se…Se diagonals, which range between 5.56(2) and 5.716(7) Å, despite the absence of similar packing effects.

Chemical mono-oxidation of **1**^{iPr}-H_6 disrupts the π-π network and increases its solubility. [Co_6Se_8] clusters exhibit very rich redox profiles, undergoing up to four reversible single-electron oxidations.[44] Indeed, treating a slurry of **1**^{iPr}-H_6 in THF with ferrocenium hexafluorophosphate ($FcPF_6$; 1 equiv) causes an immediate dissolution of the suspended solids, and is associated with a simultaneous change in color from red-brown to a deep red-orange hue. The mixture was stirred for 1 h before volatiles were removed *in vacuo*, and the resulting solids were slurried in toluene to remove the ferrocene. The dark red oxidized cluster, [**1**^{iPr}-H_6][PF_6] (82% yield), now highly soluble in more polar solvents like acetonitrile, THF or DCM, can be easily crystallized from a mixture of THF and diethyl ether. Its ^{1}H NMR profile, recorded in d_3-acetonitrile, is comparable to that observed for **1**^{iPr}-H_6, although both the N*H* and C*H*$(CH_3)_2$ proton resonances are slightly broadened due to the S = 1/2 $Co_6Se_8^{(+)}$ core. Single crystal X-ray diffraction analysis confirms mono-oxidation (Figure 5c). In addition to the presence of the PF_6^- counterion, we note changes in bond lengths that are diagnostic of cluster mono-oxidation.[21] For example, as the intracore *trans*-Co…Co distances contract by ca. 0.08 Å from 4.197 to 4.120 Å (avg.), the Co–P bonds elongate by ca. 0.03 Å from 2.13 to 2.16 Å (avg.).

Scheme 3. Chemical oxidation of the homoleptic [Co_6Se_8] cluster, **1**^{iPr}-H_6.

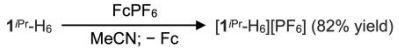

Ternary Clusters 1^{iPr}-M_3 (M = Fe, Zn)

To trimetallate **1**^{iPr}-H_6, we adapted the previously reported protocol (**Error! Reference source not found.**).[11] To ensure the quantitative hexadeprotonation of **1**^{iPr}-H_6, a solvent mixture of PhCl and THF (5:1) and excess ^{n}BuLi (8 equiv) were used. ^{31}P NMR analysis indicates that complete deprotonation is associated with a 10 ppm upfield shift in the signal of the amidophosphine phosphorus, to 89 ppm. In contrast to **1**^{Tol}-H_6, the hexalithiated species, tentatively identified as $Li_6(THF)_xCo_6Se_8L_6$ (**1**^{iPr}-$Li_6(THF)_x$), does not precipitate from the PhCl solution, yet aliquots collected from the deprotonation mixture could not be redissolved in benzene-d_6 after removal of solvent. Trimetallation was achieved in situ in the stoichiometric reaction between the hexalithiated complex **1**^{iPr}-$Li_6(THF)_x$ and MCl_2 (M = Fe, Zn; **Error! Reference source not found.**). Crude NMR spectroscopy analysis indicated the formation of a one major product, **1**^{iPr}-M_3. Significantly more soluble than their parent metalloligand, the **1**^{iPr}-M_3 clusters can be isolated pure in good yields by crystallization (76 and 77% yield for Fe, and Zn, respectively). Compared to the tolyl derivative **1**^{Tol}-Fe_3, the **1**^{iPr}-M_3 clusters are highly water sensitive, forming **1**^{iPr}-H_6, or a mixture of mono- and dimetallated clusters in the presence of trace water. Intrigued at the possibility to access the putative zwitterion [**1**^{iPr}-$Li_6(THF)_x$][PF_6], we found that the hexadeprotonation of the mono-oxidized cluster [**1**^{iPr}-H_6][PF_6] produces a mixture of species instead. Among them, a major component is neutral **1**^{iPr}-H_6, presumably formed by chemical reduction of [**1**^{iPr}-H_6][PF_6] by ^{n}BuLi.

Scheme 4. Synthesis of trimetallated nanopropellers **1**^{iPr}-Fe_3 and **1**^{iPr}-Zn_3.

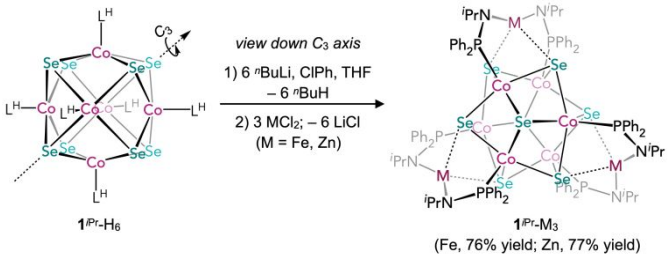

Single crystal X-ray analysis of **1**^{iPr}-M_3 reveals that they crystallize with no solvents coordinated to the edge sites (Figure 6), in contrast to **1**^{Tol}-Fe_3 which was only obtained in single crystal form only as a solvent adduct.[11] As a result of the κ^4 chelation of M by the metallocluster, the inorganic $M_3Co_6Se_8$ cores of **1**^{iPr}-M_3 exhibit near-perfect D_3 symmetry. Structurally, this resembles closest

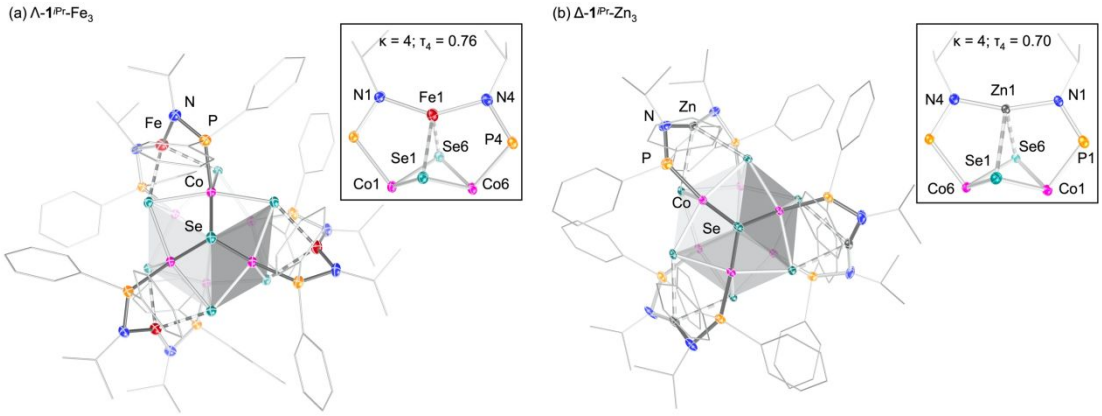

Figure 6. Single crystal X-ray structures of the nanopropeller clusters, Λ-**1**^{iPr}-Fe_3 (a) and Δ-**1**^{iPr}-Zn_3 (b), with insets highlighting the κ^4-bound edge sites. (a) Selected interatomic distances (Å): (a) Fe1–Se1 2.5360(2), Fe1–Se6 2.496(2), Fe1–N1 1.962(2), Fe1–N4 1.952(4), Fe1–Co1 2.885(1), Fe1–Co6 2.831(2), Co1–Co6 2.780(5), Co1–Se1 2.373(2), Co6–Se6 2.401(2), Co6–P4 2.171(2), P4–N4 1.6512(6); (b) Zn1–Se1 2.711(2), Zn1–Se6 2.660(5), Zn1–N1 1.882(7), Zn1–N4 1.888(8), Zn1–Co1 3.181(4), Zn1–Co6 3.181(3), Co1–Co6 2.910(4), Co1–Se1 2.369(2), Co6–Se6 2.385(1), N1–P1 1.648(8), Co1–P1 2.163(3). For Δ-**1**^{iPr}-Zn_3, plotted is only the major component (88% occupancy), omitting for clarity the cocrystallizing **1**^{iPr}-H_6 (12% occupancy; see S4.7). Thermal ellipsoids plotted at 50% probability. Hydrogen atoms, co-crystallizing solvent, and disorder are omitted. All carbon atoms are displayed as wireframes for clarity.

the previously reported monoreduced cluster $[\mathbf{1}^{Tol}\text{-}Fe_3]^-$, isolated and characterized in the solid state free of bound surface ligands.[11] As was the case for $[\mathbf{1}^{Tol}\text{-}Fe_3]^-$, the $M_3Co_6Se_8$ units of $\mathbf{1}^{iPr}\text{-}M_3$ can be deconstructed into three (μ_4-Se)-bicapped trinuclear MCo_2 subunits interconnected along their Co…Co edge by two apical, non-M binding μ_3-Se atoms, which also define the principle C_3 rotational axis of the cluster. Similarly to the tolyl derivatives, $\mathbf{1}^{iPr}\text{-}M_3$ crystallize as a racemic mixture of helical (Δ/Λ)-enantiomers.

In $\mathbf{1}^{iPr}\text{-}Fe_3$, each Fe edge site is bound κ^4 by the metalloligand via two amides and two μ_4-Se atoms, giving rise to a distorted-tetrahedral coordination at iron (τ_4 = 0.76; Figure 6a).[45] The six Fe–Se bonds range between 2.496(2) and 2.5360(2) Å,[46] and cause pronounced structural distortions within the Co_6Se_8 cluster core. For example, the Co–(μ_4-Se) distances of 2.38 Å (avg.) are significantly longer than the Co–(μ_3-Se) bonds of 2.33 Å (avg.). This elongation effectively flattens the Co_6Se_8 cube in the equatorial plane defined by the edge sites. This distortion can be quantified by the differences between the axial (along the C_3 axis) and equatorial Se...Se diagonal distances of the Co_6Se_8 core, of 5.412(8) and 5.77 (avg.) Å, respectively. Additionally, the Fe…Co and Co…Co interatomic distances within the $FeCo_2$ subunits average 2.87 and 2.80 Å, respectively, whereas the Co…Co distances that separate these triangles average 3.00 Å. These trends are similar to those observed for $[\mathbf{1}^{Tol}\text{-}Fe_3]^-$, although in $\mathbf{1}^{iPr}\text{-}Fe_3$ the Fe–Se contacts are slightly longer (2.52 vs 2.46 Å, avg.), and the core distortions are slightly less pronounced. While a direct comparison of bonding metrics with the neutral $\mathbf{1}^{Tol}\text{-}Fe_3$ cluster cannot be made since the latter was crystallized only as the tris-adduct $\mathbf{1}^{Tol}\text{-}Fe_3(CN^tBu)_3$, we note that the three Fe–Se bonds in neutral tolyl cluster $\mathbf{1}^{Tol}\text{-}Fe_3$, averaging 2.51, are comparable to 2.52 Å, the average value for the six Fe–Se bonds in $\mathbf{1}^{iPr}\text{-}Fe_3$.[11]

The trizinc variant $\mathbf{1}^{iPr}\text{-}Zn_3$ exhibits a similar structure, except the Zn(II) sites coordinate in a geometry better described as distorted seesaw than tetrahedral ($\theta_{N\text{-}Zn\text{-}N} \approx 161°$; τ_4 = 0.70). Compared to $\mathbf{1}^{iPr}\text{-}Fe_3$, the edge-support interactions in $\mathbf{1}^{iPr}\text{-}Zn_3$ are weaker, as reflected by weak Zn–Se bonds, ranging in length between 2.648(2) and 2.780(4) Å.[47] Consequently, the structural distortion of the Co_6Se_8 core is also less pronounced, with roughly equivalent axial and equatorial Se…Se diagonals of 5.613(4) and 5.66 (avg.) Å, respectively.

The electronic changes brought about by replacing the tolyl substituents with isopropyl ones in the $\mathbf{1}^{iPr}\text{-}M_3$ clusters was probed in solution using UV-vis-*n*IR absorption spectroscopy and cyclic voltammetry (Figure 7). A comparison of the electronic absorption profile of $\mathbf{1}^{iPr}\text{-}Fe_3$ with that of $\mathbf{1}^{Tol}\text{-}Fe_3$, collected in a non-coordinative solvent (toluene), where no surface ligands are bound to either of the two clusters, reveals the main absorption feature of the isopropyl derivative is blue-shifted by 16 nm, and slightly less intense than that of the tolyl derivative (Figure 7a). We also note that while trimetallation with Fe perturbs significantly the characteristic absorption features of the metalloligand, this is less pronounced in the Zn derivative, empirically proportional to the degree of structural distortion observed within the Co_6Se_8 core. While the three absorption bands of $\mathbf{1}^{iPr}\text{-}Zn_3$ are red-shifted and broadened relative to those of $\mathbf{1}^{iPr}\text{-}H_6$, they are centered at a similar energy to the broad feature of $\mathbf{1}^{iPr}\text{-}Fe_3$.

Cyclic voltammetry reveals that both ternary $\mathbf{1}^{iPr}\text{-}M_3$ clusters feature a total of five pseudo-reversible one-electron redox processes, spanning oxidation states between –2 and +3 (Figure 7b). We note that the HOMO-LUMO gap, approximated as the separation between the (–1/0) and (0/+1) redox couples in THF, is smaller for $\mathbf{1}^{iPr}\text{-}Fe_3$ (1.01 eV) compared to the zinc variant $\mathbf{1}^{iPr}\text{-}Zn_3$ (1.38 eV), in accordance with the relative strength of the edge-support interactions in the two species. A comparison between the

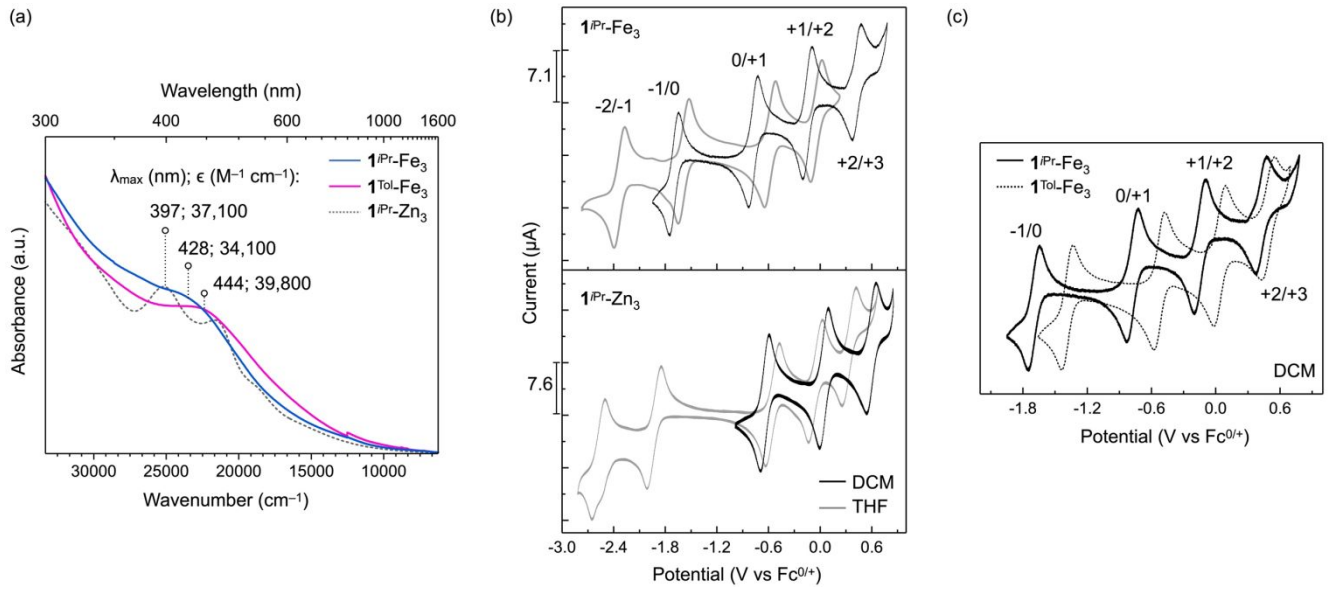

Figure 7. (a) UV-vis-*n*IR spectra including the λ_{max} (nm) and corresponding extinction coefficient ε (M^{-1} cm^{-1}) for $\mathbf{1}^{iPr}\text{-}Fe_3$ (428; 34,100), $\mathbf{1}^{Tol}\text{-}Fe_3$ (444, 39,800) and $\mathbf{1}^{iPr}\text{-}Zn_3$ (397; 37,100), acquired in toluene. (b) Cyclic voltammograms of $\mathbf{1}^{iPr}\text{-}Fe_3$ and $\mathbf{1}^{iPr}\text{-}Zn_3$ recording in DCM or THF (0.1 M $TBAPF_6$) at 50 mV/s. (c) Comparison between the electrochemical profiles of $\mathbf{1}^{iPr}\text{-}Fe_3$ and $\mathbf{1}^{Tol}\text{-}Fe_3$, acquired in DCM (0.1 M $TBAPF_6$) at 50 mV/s.

electrochemical profiles of $\mathbf{1}^{i\mathrm{Pr}}$-$Fe_3$ and $\mathbf{1}^{\mathrm{Tol}}$-$Fe_3$ carried out in a DCM, a non-coordinative solvent, reveals an overall shift of the redox events to more reducing potentials (Figure 7c).[11] This change is in line with the more electron rich character of the isopropyl groups of $\mathbf{1}^{i\mathrm{Pr}}$-$Fe_3$ compared to the tolyl substituents in $\mathbf{1}^{\mathrm{Tol}}$-$Fe_3$. Another difference is a widening of the HOMO/LUMO gap in the isopropyl derivative compared to the tolyl one ((0.92 vs 0.87 eV in DCM). The decreased stabilization of the LUMO level can be attributed to the diminished Lewis acidity of the Fe sites in $\mathbf{1}^{i\mathrm{Pr}}$-$Fe_3$, which is also corroborated by coordination studies with CN^{t}Bu (see below).

In solution, NMR analysis reveals that the free rotation of the isopropyl substituents at the Fe and Zn edges is hindered. For example, $\mathbf{1}^{i\mathrm{Pr}}$-$Fe_3$ exhibits a total of eight paramagnetic proton resonances between 20 and –20 ppm, more than the five expected for a freely rotating ligand environment (Figure S16). As observed for $\mathbf{1}^{\mathrm{Tol}}$-$Fe_3$, the ligand framework in $\mathbf{1}^{i\mathrm{Pr}}$-$M_3$ is locked, both in the solid state and in solution, in a helical conformation, such that two phenyl groups of each phosphine adopt either an axial or equatorial orientation, giving rise to two separate sets of NMR resonances. However, ^{1}H integrations for $\mathbf{1}^{i\mathrm{Pr}}$-$Fe_3$ suggest that the ^{i}Pr-C*H*$_3$ groups are also resolved under D_3 symmetry, indicating that the isopropyl substituents are sterically locked in place at the edge sites. In contrast, the tolyl substituents in $\mathbf{1}^{\mathrm{Tol}}$-$Fe_3$ rotate freely even in a non-coordinative solvent, as is reflected by the singular set of tolyl resonances in its ^{1}H NMR profile.[11] Noteworthy, solution-phase magnetic measurements carried out using the Evans method[48] confirm the iron edge sites remain high spin (S = 2) in $\mathbf{1}^{i\mathrm{Pr}}$-$Fe_3$ (μ_{eff} = 9.4 μ_B), as was observed for $\mathbf{1}^{\mathrm{Tol}}$-$Fe_3$.[11] In the trizinc variant, $\mathbf{1}^{i\mathrm{Pr}}$-$Zn_3$ the desymmetrization associated with the hindered rotation is reflected in both its ^{1}H and ^{13}C NMR spectra, for example by the presence of additional proton features in the aromatic region, and two nearly overlapping sets of ^{i}Pr-C*H*$_3$ and ^{i}Pr-C*H* resonances (Figures S17 and S18).

Comparison of space filling models for $\mathbf{1}^{i\mathrm{Pr}}$-$Fe_3$ and $[\mathbf{1}^{\mathrm{Tol}}\text{-}Fe_3]^-$,[11] both featuring edge sites coordinated κ^4 by the metalloligand, reveals indeed the presence of the required space to allow the rotation of the tolyl groups, whereas the increased steric bulk of the isopropyl substituents appear to keep them locked in $\mathbf{1}^{i\mathrm{Pr}}$-$Fe_3$ (Figure 8). An important implication of the increased steric bulk at the edge Fe sites is that it might be a leading factor in preventing coordination of sufficiently large ligands. We set out to probe the affinity for ligands of the edge sites in $\mathbf{1}^{i\mathrm{Pr}}$-$Fe_3$, and compare it to those in $\mathbf{1}^{\mathrm{Tol}}$-$Fe_3$. Treatment of $\mathbf{1}^{i\mathrm{Pr}}$-$Fe_3$ with THF, or excess pyridine (15 equiv) in benzene-d_6 revealed little to no changes in its paramagnetic ^{1}H resonances, consistent with no binding interactions (Figure S24). This resembles the behavior of the edge sites in the monoreduced $[\mathbf{1}^{\mathrm{Tol}}\text{-}Fe_3]^-$ cluster, but stands in contrast to the neutral $\mathbf{1}^{\mathrm{Tol}}$-$Fe_3$ which coordinates in solution to both.[11] To probe if the zero affinity of $\mathbf{1}^{i\mathrm{Pr}}$-Fe for these solvents is sterically enforced, we turned to the trimmer CN^{t}Bu ligand, known to bind to $\mathbf{1}^{\mathrm{Tol}}$-$Fe_3$, but not to the monoreduced cluster $[\mathbf{1}^{\mathrm{Tol}}\text{-}Fe_3]^-$. Treatment of $\mathbf{1}^{i\mathrm{Pr}}$-$Fe_3$ with CN^{t}Bu (15 equiv) elicited subtle, but noticeable changes in its proton chemical shifts, suggesting coordinative interactions. The CN infrared stretch of the coordinated isocyanide (ν_{CN} = 2104 cm^{-1}), acquired after removal of the unbound excess ligand, is red-shifted compared to both free CN^{t}Bu and $\mathbf{1}^{\mathrm{Tol}}$-$Fe_3(CN^t\mathrm{Bu})_3$ (ν_{CN} = 2167, 2141 cm^{-1}, respectively; Figure 9). In contrast to the neutral $\mathbf{1}^{\mathrm{Tol}}$-$Fe_3$ where the electron deficient Fe sites not only do not activate the isocyanide, but form one of the most deactivated adduct to be reported,[11] in $\mathbf{1}^{i\mathrm{Pr}}$-$Fe_3$ the edge sites are sufficiently electron rich to participate in backbonding with this π-acceptor, ostensibly due to the increased donor strength of the isopropyl amido ligands.

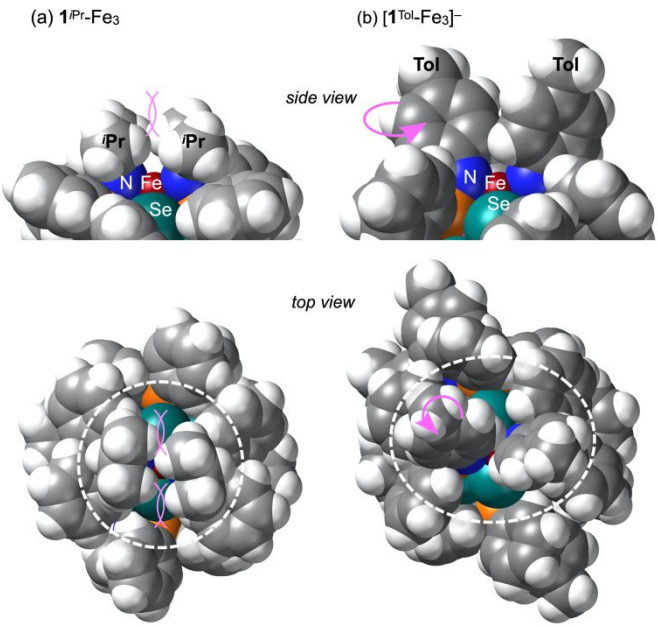

Figure 8. Space filling models for a single κ^4–Fe edge site in (a) $\mathbf{1}^{i\mathrm{Pr}}$-$Fe_3$ and (b) $[\mathbf{1}^{\mathrm{Tol}}\text{-}Fe_3]^-$, including a zoom-in on the side view, highlighting the isolated edge site, and the full cluster viewed from the top of the outlined edge site.

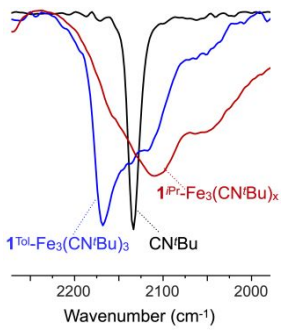

Figure 9. Comparison of CN infrared stretches of free CN^{t}Bu (black), $\mathbf{1}^{\mathrm{Tol}}$-$Fe_3(CN^t\mathrm{Bu})_3$ (blue) and $\mathbf{1}^{i\mathrm{Pr}}$-$Fe_3(CN^t\mathrm{Bu})_x$ (red).

Conclusions

The ternary clusters $\mathbf{1}^{\mathrm{R}}$-M_3 introduced by our group provide a new strategy to access redox-active multimetallic platforms with synthetically addressable, and hemilabile active sites. In previous work we demonstrated that not only the oxidation state of the overall cluster,[11] but also the chemical identity of

the edge sites[12] provide a mechanism to tune their affinity to bind additional ligands (e.g. pyridine or CN^{t}Bu). In this report we probed the effects of small alterations in the stereoelectronic properties of the aminophosphine ligands, and found they significantly alter the [Co_6Se_8] cluster formation process, in addition to their affinity for external ligands and the strength of the edge/support interaction in **1**^{iPr}-M_3. While a slight increase in the steric bulk of the substituents of the amido groups that anchor the edge metals on the inorganic cobalt core appears to be the primary factor modulating ligand coordination, their increased donor strength was found to also contribute to the resulting electronic properties of the ternary clusters. In conclusion, we demonstrate how small modifications in the ligand framework of the ternary nanopropeller clusters **1**^{R}-M_3 can result in pronounced impacts on their coordinative and physical properties, altering the push-pull dynamic between the [Co_6Se_8] support, the edge metal and external coordinating ligands.

Conflicts of interest

There are no conflicts to declare.

Acknowledgements

This research was supported by the University of Washington by startup funds, by a Royal Research Fund (RRF) grant, and by the National Science Foundation (NSF) through a Faculty Early Career Development Program award. The authors thank Dr. M. Blakely and D. Rogers for additional assistance with X-ray crystallography, and Dr. A. Chirila for helpful suggestions.

References

1 I. Bertini, Ed., *Biological inorganic chemistry: structure and reactivity*, University Science Books, Sausalito, Calif, 2007.
2 N. Cox, M. Retegan, F. Neese, D. A. Pantazis, A. Boussac and W. Lubitz, *Science*, 2014, **345**, 804–808.
3 R. M. Bullock, J. G. Chen, L. Gagliardi, P. J. Chirik, O. K. Farha, C. H. Hendon, C. W. Jones, J. A. Keith, J. Klosin, S. D. Minteer, R. H. Morris, A. T. Radosevich, T. B. Rauchfuss, N. A. Strotman, A. Vojvodic, T. R. Ward, J. Y. Yang and Y. Surendranath, *Science*, 2020, **369**, eabc3183.
4 D. Coucouvanis, P. E. Mosier, K. D. Demadis, S. Patton, S. M. Malinak, C. G. Kim and M. A. Tyson, *J. Am. Chem. Soc.*, 1993, **115**, 12193–12194.
5 F. Li, R. L. Meyer, S. H. Carpenter, L. E. VanGelder, A. W. Nichols, C. W. Machan, M. L. Neidig and E. M. Matson, *Chem. Sci.*, 2018, **9**, 6379–6389.
6 G. de Ruiter, K. M. Carsch, S. Gul, R. Chatterjee, N. B. Thompson, M. K. Takase, J. Yano and T. Agapie, *Angew. Chem.*, 2017, **129**, 4850–4854.
7 A. I. Nguyen, L. E. Darago, D. Balcells and T. D. Tilley, *J. Am. Chem. Soc.*, 2018, **140**, 9030–9033.
8 J. S. Kanady, P.-H. Lin, K. M. Carsch, R. J. Nielsen, M. K. Takase, W. A. Goddard and T. Agapie, *J. Am. Chem. Soc.*, 2014, **136**, 14373–14376.
9 S. Mukherjee, J. A. Stull, J. Yano, T. C. Stamatatos, K. Pringouri, T. A. Stich, K. A. Abboud, R. D. Britt, V. K. Yachandra and G. Christou, *Proc. Natl. Acad. Sci.*, 2012, **109**, 2257–2262.
10 C. Zhang, C. Chen, H. Dong, J.-R. Shen, H. Dau and J. Zhao, *Science*, 2015, **348**, 690–693.
11 J. A. Kephart, B. S. Mitchell, A. Chirila, K. J. Anderton, D. Rogers, W. Kaminsky and A. Velian, *J. Am. Chem. Soc.*, 2019, **141**, 19605–19610.
12 J. A. Kephart, C. G. Romero, C.-C. Tseng, K. J. Anderton, M. Yankowitz, W. Kaminsky and A. Velian, *Chem. Sci.*, 2020, 10.1039.D0SC03506H.
13 B. P. Greenwood, S. I. Forman, G. T. Rowe, C.-H. Chen, B. M. Foxman and C. M. Thomas, *Inorg Chem*, 2009, **48**, 6251–6260.
14 C. A. Tolman, *Chem. Rev.*, 1977, **77**, 313–348.
15 L. Falivene, Z. Cao, A. Petta, L. Serra, A. Poater, R. Oliva, V. Scarano and L. Cavallo, *Nat. Chem.*, 2019, **11**, 872–879.
16 D. Fenske, J. Hachgenei and J. Ohmer, *Angew. Chem. Int. Ed.*, 1985, **24**, 706–709.
17 D. Fenske, J. Ohmer and J. Hachgenei, *Angew. Chem. Int. Ed.*, 1985, **24**, 993–995.
18 D. Fenske, J. Ohmer and K. Merzweiler, *Z. Für Naturforschung B*, 1987, **42**, 803–809.
19 M. L. Steigerwald, T. Siegrist and S. M. Stuczynski, *Inorg. Chem.*, 1991, **30**, 2256–2257.
20 S. M. Stuczynski, Y. U. Kwon and M. L. Steigerwald, *J. Organomet. Chem.*, 1993, **449**, 167–172.
21 B. Choi, J. Yu, D. W. Paley, M. T. Trinh, M. V. Paley, J. M. Karch, A. C. Crowther, C.-H. Lee, R. A. Lalancette, X. Zhu, P. Kim, M. L. Steigerwald, C. Nuckolls and X. Roy, *Nano Lett.*, 2016, **16**, 1445–1449.
22 A. M. Champsaur, J. Yu, X. Roy, D. W. Paley, M. L. Steigerwald, C. Nuckolls and C. M. Bejger, *ACS Cent. Sci.*, 2017, **3**, 1050–1055.
23 X. Roy, C. L. Schenck, S. Ahn, R. A. Lalancette, L. Venkataraman, C. Nuckolls and M. L. Steigerwald, *Angew. Chem. Int. Ed.*, 2012, **51**, 12473–12476.
24 M. L. Steigerwald, T. Siegrist and S. M. Stuczynski, *Inorg. Chem.*, 1991, **30**, 4940–4945.
25 A. M. Champsaur, A. Velian, D. W. Paley, B. Choi, X. Roy, M. L. Steigerwald and C. Nuckolls, *Nano Lett.*, 2016, **16**, 5273–5277.
26 C. A. Tolman, *J. Am. Chem. Soc.*, 1970, **92**, 2953–2956.
27 J. Jover and J. Cirera, *Dalton Trans.*, 2019, **48**, 15036–15048.
28 F. A. Cotton, C. A. Murillo and R. A. Walton, Eds., *Multiple Bonds Between Metal Atoms*, Springer-Verlag, New York, 2005.
29 L. Pauling, *J. Am. Chem. Soc.*, 1947, **69**, 542–553.
30 N. Casati, P. Macchi and A. Sironi, *Angew. Chem.*, 2005, **117**, 7914–7917.
31 P. N. Bungu and S. Otto, *Dalton Trans.*, 2011, **40**, 9238.

32 J. M. Birbeck, A. Haynes, H. Adams, L. Damoense and S. Otto, *ACS Catal.*, 2012, **2**, 2512–2523.
33 L. Markó, G. Bor, E. Klumpp, B. Markó and G. Almásy, *Chem. Ber.*, 1963, **96**, 955–964.
34 G. Gervasio, S. F. A. Kettle, F. Musso, R. Rossetti and P. L. Stanghellini, *Inorg. Chem.*, 1995, **34**, 298–305.
35 G. Gervasio, R. Rossetti, P. L. Stanghellini, D. Braga and S. F. A. Kettle, *J. Crystallogr. Spectrosc. Res.*, 1993, **23**, 255–264.
36 A. D. Harley, G. J. Guskey and G. L. Geoffroy, *Organometallics*, 1983, **2**, 53–59.
37 M. L. H. Green, *J. Organomet. Chem.*, 1995, **500**, 127–148.
38 C. E. Strouse and L. F. Dahl, *J. Am. Chem. Soc.*, 1971, **93**, 6032–6041.
39 S. Vastag, G. Gervasio, D. Marabello, G. Szalontai and L. Markó, *Organometallics*, 1998, **17**, 4218–4225.
40 J. E. Davies, M. J. Mays, P. R. Raithby, V. Sarveswaran and G. P. Shields, *J. Chem. Soc. Dalton Trans.*, 1998, 775–780.
41 A. J. Edwards, A. Martían, M. J. Mays, D. Nazar, P. R. Raithby and G. A. Solan, *J Chem Soc Dalton Trans*, 1993, 355–363.
42 R. Hernández Sánchez, A. M. Champsaur, B. Choi, S. G. Wang, W. Bu, X. Roy, Y. Chen, M. L. Steigerwald, C. Nuckolls and D. W. Paley, *Angew. Chem. Int. Ed.*, 2018, **57**, 13815–13820.
43 Z.-F. Yao, J.-Y. Wang and J. Pei, *Cryst. Growth Des.*, 2018, **18**, 7–15.
44 A. Turkiewicz, D. W. Paley, T. Besara, G. Elbaz, A. Pinkard, T. Siegrist and X. Roy, *J. Am. Chem. Soc.*, 2014, **136**, 15873–15876.
45 L. Yang, D. R. Powell and R. P. Houser, *Dalton Trans*, 2007, 955–964.
46 *A search for all Fe...Se bond lengths in the Cambridge Structural Database (updated June 2020) yielded 591 hits between 2.142 and 2.949 Å (mean 2.39(6) Å).*, .
47 *A search for all Zn...Se bond lengths in the Cambridge Structural Database (updated June 2020) yielded 140 hits between 2.289 and 2.949 Å (mean 2.47(7) Å).*, .
48 D. F. Evans, *J. Chem. Soc. Resumed*, 1959, 2003.

Subtle stereoelectronic changes of the surface capping ligands have long-ranging consequences in the synthesis and chemistry of ternary transition metal selenide clusters.

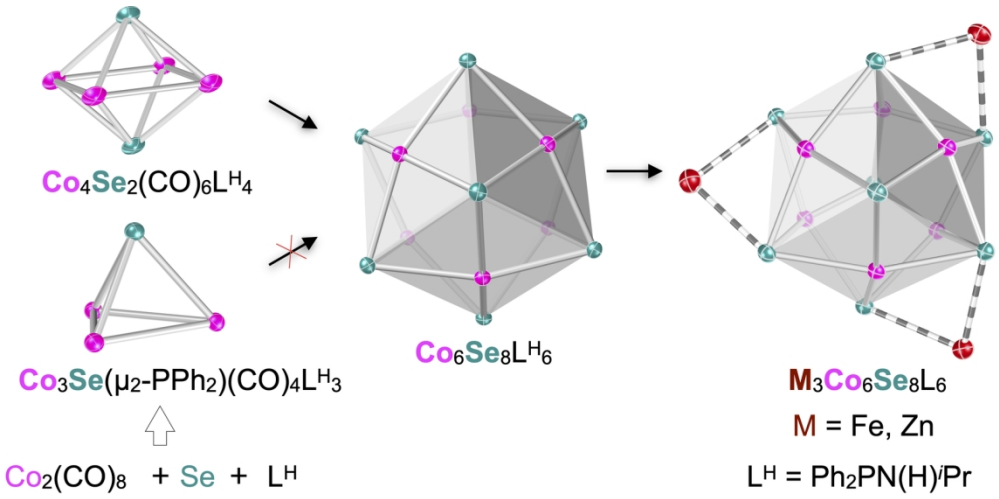

76x37mm (600 x 600 DPI)